IEEE Access
Multidisciplinary : Rapid Review : Open Access Journal

Received 17 October 2023, accepted 7 November 2023, date of publication 9 November 2023, date of current version 15 November 2023.

Digital Object Identifier 10.1109/ACCESS.2023.3331815

RESEARCH ARTICLE

Intelligent Real-Time Image Processing Technology of Badminton Robot via Machine Vision and Internet of Things

BIN LIU[1] AND YINGYING ZHENG[2]
[1]School of Computer Science, Taylor's University, Subang Jaya, Selangor 47500, Malaysia
[2]College of Physical Education and Health, Wenzhou University, Wenzhou 325035, China

Corresponding author: Yingying Zheng (Zjzyy881@sina.com)

ABSTRACT The development of precise detection and tracking methods for high-speed moving targets, coupled with accurate matching under varying lighting conditions, represents a formidable challenge in the realm of badminton robot creation. To tackle these intricate issues, this work introduces a suite of innovative techniques within the domain of intelligent robot image processing, offering substantial impetus to the evolution of badminton robots. Primarily, the work designs a high-precision binocular stereo vision acquisition system to enhance the accurate reconstruction of the badminton shuttlecock's trajectory in three-dimensional space, enabling real-time monitoring and in-depth analysis of shuttlecock motion. Subsequently, an inventive dynamic threshold Gaussian mixture model, underpinned by singular value decomposition, is introduced. This model dynamically adjusts the decision threshold based on background-foreground similarity while ensuring synchronized exposure between the left and right cameras and timely data retrieval. Lastly, the study addresses the impact of lighting fluctuations on target matching through a Retinex-based color histogram matching method, adapting color histogram templates according to varying lighting intensities. Experimental validation involves the utilization of an industrial digital camera with frame exposure to capture badminton images, subsequently transforming image processing into motion control to effectively realize the badminton robot's hitting action. The experimental outcomes highlight the following achievements: 1) The designed badminton robot achieves a remarkable 100% recognition rate for the shuttlecock under normal conditions, featuring a standard deviation of θ below 0.05°, a position standard deviation of less than 18 millimeters in the x-axis direction, and less than 8 millimeters in the y-axis direction; 2) The proposed binocular stereo vision acquisition system exhibits superior precision, profoundly supporting shuttlecock trajectory analysis; 3) The Gaussian mixture model, incorporating dynamic threshold adjustment via singular value decomposition, excels in detecting delicate and diminutive moving targets, showcasing high-level detection accuracy. These experimental findings offer novel insights into the domain of intelligent real-time image processing technology for badminton robots anchored in the IoT (Internet of Things) machine vision. The implications reverberate through the further advancement of badminton robots, charting a novel technical trajectory that amalgamates intelligent real-time image processing with the IoT. Consequently, the amalgamation bolsters hitting accuracy and motion performance, cohering with the ongoing trajectory of robotics technology development, which emphasizes the integration of intelligence and autonomy across diverse facets of robotics. This alignment propels continuous progress throughout the entire expanse of robotics technology.

INDEX TERMS Internet of Things, machine vision, badminton robots, real-time image processing.

The associate editor coordinating the review of this manuscript and approving it for publication was Qichun Zhang.

© 2023 The Authors. This work is licensed under a Creative Commons Attribution-NonCommercial-NoDerivatives 4.0 License.
For more information, see https://creativecommons.org/licenses/by-nc-nd/4.0/

I. INTRODUCTION

Badminton is the second popular sport among Chinese nationals. However, it is often difficult for people to find suitable venues and companions for badminton with specific requirements. Therefore, a badminton robot is necessary to solve these problems and greatly enhance the badminton fun [1]. In addition, it can promote the participation of all people in badminton, increase the duration of sports of people, and enhance the influence of badminton [2]. The robot is an automated and highly flexible machine with intellectual abilities similar to those of human beings or other creatures, such as planning, perception, action, and coordination [3]. A dozen years ago, the limited robot technology could only perform the fixed procedures preset by human beings, which was hard to contend with [4]. When people believed that robots could not conquer human beings in chess as always, in 2016, "Alpha Go" of Google Inc. beat Lee Se-dol with the final score of 4-1, which undoubtedly hit human beings in the head with a brick [5]. Since then, sensors, processor technology, and even artificial intelligence have made significant progress, and automated driving technology has also been applied in mass production. Table tennis robots are the earlier application of robots in sports, which have reached the level of confrontation practice with professional athletes [6]. Scholars have also developed research on badminton robots, about the global design of badminton robots and a particular function of badminton, among which the most crucial part is three-dimensional visual acquisition [7]. The three-dimensional visual acquisition is widely used in ball robots, including badminton robots, football robots, and table tennis robots [8]. The three-dimensional visual acquisition has also been commonly used in sports competition analysis and referee's decision, like the well-known Hawk-Eye-Instant playback system in tennis. The current three-dimensional vision acquisition technology generally includes monocular stereo vision acquisition, binocular stereo vision acquisition, and depth camera [9]. As the name implies, the binocular stereo vision system simulates human vision using two cameras. It obtains the three-dimensional geometric data of the measured object according to the parallax principle [10]. Similarly, the technology is widely used in various sports robots [11].

The real-time image processing of badminton trajectory based on the machine vision of the IoT (Internet of Things) adopts binocular stereo vision technology, fast-moving object recognition, and trajectory prediction, which all have practical application values in various fields such as industry, civil industry, and national defense. It is innovative to independently design the high-precision binocular stereo vision acquisition system and propose the Gaussian mixture model based on dynamic decomposition threshold adjustment. Moreover, a series of problems in badminton sports for badminton enthusiasts are solved, such as no partner, time coordination, and venue coordination. Therefore, groundbreaking research improves national participation in badminton, increases the duration of national sports, and enhances the physique of the overall people.

Researchers have also gained many research achievements in the field of visual technology. In the field of target detection, Li et al. [12] pointed out that litchi clusters in orchards were randomly dispersed and irregularly distributed. Hence, it was difficult to detect and locate the fruiting branches of multiple litchi clusters at the same time. Therefore, the authors developed a reliable algorithm based on an RGB-Deep camera to accurately and automatically detect and locate the fruiting branches of multiple litchi clusters in a large environment. In this project, the author proposed a pre-processing step to align the segmented RGB image and remove the unfruitful branches, and a noise application spatial clustering method based on nonparametric density to cluster the pixels in the three-dimensional space of the branch skeleton image. Finally, they conducted three-dimensional linear fitting for each cluster through principal component analysis. The linear information corresponded to the position of the fruiting branch. The experimental results showed that the detection accuracy of litchi fruit was 83.33%, the positioning accuracy was $17.29° \pm 24.57°$, and the detection execution time of single litchi fruit was 0.464 seconds. Guo et al. [13] proposed an overlapping detection method for litchi fruit based on monocular machine vision. Specifically, they combined the contrast-constrained adaptive histogram equalization, red/blue color mapping, Otsu threshold, and morphological operation to segment the foreground area of litchi. Besides, they explored a step-by-step method for extracting litchi fruit individuals from the foreground area of litchi. The authors collected 485 images from a natural litchi orchard in the Conghua District of Guangzhou and evaluated the performance of this method. The test results indicated that the recall rate was 86.66 %, the accuracy rate was more than 87 %, and the F1-score was 87.07 %. In the field of 3D reconstruction, Chen et al. [14] integrated hand-eye stereo vision and the simultaneous localization and mapping system to provide detailed global maps supporting long-term, flexible, and large-scale orchard harvesting. The authors also designed a mobile robot based on hand-eye vision, proposed an effective hand-eye calibration method, trained an advanced target detection network, and built a dynamic stereo matching method adapted to a complex orchard environment. The experimental results demonstrated that the global map constructed by the author realized a large scale and high resolution. Song et al. [15] utilized DeepLabV3+ to slice the calyx, branch and silk of the fruit and proposed a discrete line pixel reconstruction method based on progressive probability Hough transform to detect line distribution. They proved that the correct detection rate of the proposed algorithm was 92.4% through experiments, and the processing time was 6.4 ms/image, which was competitive. However, the authors thought there were still some shortcomings in the research work, which needed to be continuously improved and innovated to obtain stronger

robustness and broader adaptability. Moreover, as one of the primary and critical links in the field of robot vision, motion object detection still faced the problem of low recognition rate under the conditions of illumination change, camera jitter, and object movement in the background. To sum up, correlation filtering algorithms and DL (deep learning) algorithms are the mainstream visual target tracking algorithms. Due to the high computational complexity of DL tracking algorithms, they usually run on the high-performance GPU, while correlation filtering algorithms have good accuracy and speed balance. In recent studies, significant strides have been made in the realm of structural assessment and detection, offering innovative methodologies to bolster accuracy and automation levels. Tang et al. have introduced a pioneering approach to visual crack width measurement, employing backbone dual-scale features. This novel method aims to elevate the automation quotient within crack detection processes. Through this advancement, the precision of crack width measurements is substantially enhanced, thereby contributing to crack detection's overall accuracy and automation capacity [16]. Building on this theme, Tang et al. have delved into the seismic performance evaluation of recycled aggregate concrete-filled steel tube columns. Their work has yielded a groundbreaking, non-destructive visual technique for on-site strain detection. This innovative approach enables real-time monitoring of strain within steel tube columns, all without the need for markers. The outcome is an accurate and reliable assessment of the seismic performance of these structures [17].

Therefore, a Gaussian mixture model based on dynamic decomposition threshold adjustment update is proposed for real-time image processing of badminton trajectory, based on the IoT machine vision, binocular stereo vision technology, fast-moving object recognition technology, and trajectory prediction technology. This algorithm realizes the simple hitting of the badminton robot through the IoT machine vision technology. The research results solve a series of problems in badminton sports for badminton enthusiasts, such as difficulty in seeking a partner, coordinating time, and coordinating venues. It can also promote the participation of all people in badminton, increase the national sports time, and strengthen the overall national physique [18]. The innovation lies in a Gaussian mixture model with dynamic threshold adjustment and update based on singular value decomposition for the moving dim small targets and a color histogram matching method based on Retinex. This method overcomes the inaccurate matching results caused by different statistical results of the color histogram of the same object under different light intensities. The contribution of this work is the design of a badminton robot that can simply hit the ball using the IoT machine vision technology and the obtainment of the binocular stereo vision acquisition system with higher accuracy and matching accuracy. Under the specific experimental conditions, the badminton robot moves within Region A shown in Figure 20. In the first state, the recognition rate of the shuttlecock by the robot is 100%, the SD (standard deviation) of attitude angle θ is less than 0.05°, the SD of position in the x-axis is less than 18 mm, and the SD in the y-axis is less than 8 mm. In the second state, the recognition rate of the shuttlecock by badminton robot decreases to 95.32%, and the SD of attitude angle θ is less than 0.2°. In Region B of Figure 20, the overall recognition rate of shuttlecock by badminton robot is not less than 84.65%. By comparing the algorithm reported here with the algorithm proposed by Cao et al. [19], under the same experimental conditions, this algorithm has significantly better performance in the accuracy and attitude angle θ than that proposed by Cao et al. Moreover, through comparative analysis, the Alpha Go robot has a strong self-learning ability but poor image recognition effects. In contrast, this badminton robot integrates various image learning algorithms, such as the Gaussian mixture model of dynamic threshold adjustment and update based on singular value decomposition, and color histogram matching method based on Retinex, which to some extent makes up for the shortcomings of Alpha Go robot.

The first chapter describes the research background and significance of this work, the research results of related researchers, and an overview of the research methods. The second chapter thoroughly investigates binocular stereo vision acquisition and calibration technology, and trajectory tracking and prediction technology for moving dim small targets, and constructs the three-dimensional trajectory model and three-dimensional shuttlecock model. The third chapter adopts LMS221 laser radar technology to measure the real-time position of the badminton robot and control the movement of the badminton robot. The fourth chapter analyzes the calibration error results, threshold segmentation results, detection results, and measurement error results. The fifth chapter summarizes the present work and puts forward the outlook for future work.

The IoT technology and binocular stereo vision acquisition and calibration technology are taken as the theoretical basis for this work. Besides, fast-moving object recognition and trajectory prediction technology is employed to quickly and effectively identify the motion direction of the shuttlecock in badminton competition, and predict and judge its motion trajectory according to its motion direction. Although there are some limitations in the trajectory recognition program, it is feasible to convert vision into behavior and control the robot's badminton racket.

II. RESEARCH ON BADMINTON ROBOT TECHNOLOGY

A. ACQUISITION AND CALIBRATION OF THE BINOCULAR STEREO VISION SYSTEM

The core problem of binocular stereo vision is to understand the object or scene and its three-dimensional properties from two images in the object or scenario. The object can be moving or static. The primary task of understanding the object or scenario and its three-dimensional properties is to calibrate binocular stereo vision, since it connects the two-dimensional field of view and the three-dimensional

scenario. The binocular stereo vision system uses two or more cameras to simulate the visual system of humans or animals. It obtains the three-dimensional geometric data of the measured object by parallax principle. It has the characteristics of high accuracy, strong anti-interference, and easy installation. However, lens distortion elimination and picture line alignment are essential for the binocular stereo vision system due to imperfect camera manufacturing and installation accuracy. There are primarily five parts of the binocular stereo vision system, namely, the Gigabit Ethernet, synchronous trigger device, PC (personal computer), industrial camera, and industrial camera lens.

The binocular stereo vision system can scan the same object from two or more angles simultaneously to obtain images from different perspectives, and match the same pixels in the image. Finally, the three-dimensional spatial information of other measured objects is obtained by the system according to the principle of parallax and triangulation. Moreover, the calibration method of this system is to use the reference point coordinates and image coordinates of a given object to determine the internal and external parameters [20], [21], [22]. The internal parameters refer to the geometric and optical characteristics of the camera, including the geometric model of the camera and the distortion model of the lens. The external parameter is the coordinate relationship of the camera in the three-dimensional environment.

The parallel biaxial binocular stereo vision model is used here based on the above analysis, which has a simple structure and is easy to configure. It realizes the three-dimensional reconstruction through the time difference principle and obtains the depth information of the scene according to the triangulation method. According to the basic principle of stereo vision and the practical application purpose, the binocular stereo vision system is equipped with two industrial cameras, two optical lenses, two image acquisition cards, and a self-made optical platform (with slide rail). The size and pixel resolution of CCD (Charge-coupled Device) is 1/3 inch and 1280 × 960, respectively.

B. TRAJECTORY TRACKING AND PREDICTION OF MOVING DIM SMALL TARGETS

The moving object detection depends on machine vision, but it is the premise of trajectory tracking and prediction. The detection of fixed moving targets needs to match the characteristics of the detected moving target to those of the given target on the premise of obtaining the moving foreground to verify whether the detected target is the specified target. However, it is difficult to detect moving dim small targets because it only occupies a small number of pixels in the image with a low signal-to-noise ratio. Therefore, a Gaussian mixture model with dynamic threshold adjustment is proposed based on SVD (singular value decomposition), as well as the dynamic color histogram module matching technology based on Retinex, to test moving dim small targets. Figure 1 presents the framework of trajectory tracking and prediction of moving dim small targets.

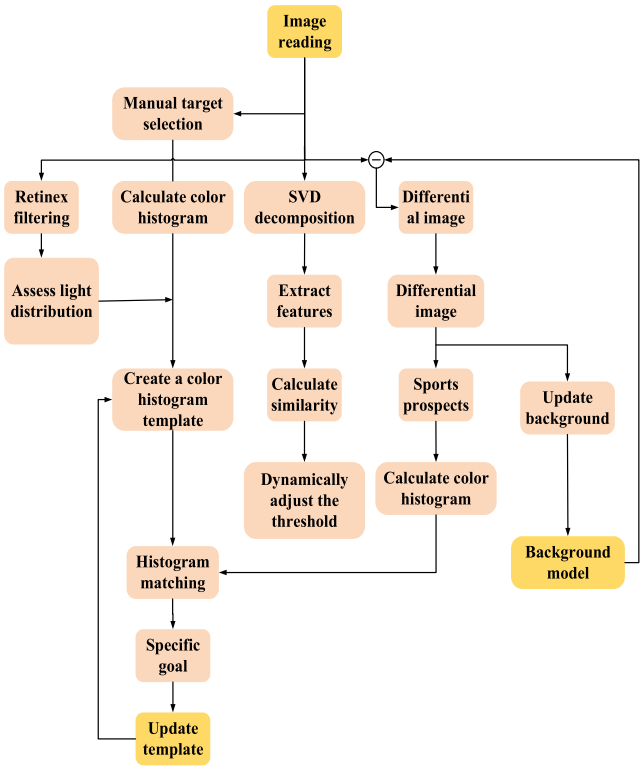

FIGURE 1. A framework of trajectory tracking and prediction of moving dim small targets.

Firstly, after reading the image, the target is manually selected for the first time. Secondly, the motion prospect, dynamic decomposition threshold, and illumination distribution of the image from the four aspects of differential image, SVD decomposition, calculation of color histogram and Retinex filtering. Besides, the color histogram is solved. Ultimately, the color histogram is matched with the corresponding template according to the specific target.

Compared with a specific probability model, the Gaussian mixture model has stronger robustness in several aspects, especially when dealing with illumination changes, slow movement, and repeated movement of situational elements. Therefore, if a pixel value in RGB or other color spaces at time t is set as $\vec{x}^{(t)}$, it can be determined whether this pixel is background or foreground according to Bayesian discrimination, as shown in Equation (1).

$$R = \frac{p(BG|\vec{x}^{(t)})}{p(FG|\vec{x}^{(t)})} = \frac{p(\vec{x}^{(t)}|BG)p(BG)}{p(\vec{x}^{(t)}|FG)p(FG)} \tag{1}$$

If $p(FG) = p(BG)$, the probability of foreground and background is the same. Meanwhile, $p(\vec{x}^{(t)}|FG) = c_{FG}$, which means that the probability distribution of foreground pixels obeys uniform distribution. Based on these, a pixel background can be determined as Equation (2).

$$p(\vec{x}^{(t)}|BG) > c_{thr}(= Rc_{FG}) \tag{2}$$

In Equation (2), c_{thr} is the discrimination threshold value, and $p(\vec{x}^{(t)}|BG)$ represents the background discrimination model. Since there may be foreground in the training set χ_T, the actual discrimination model is $p(\vec{x}^{(t)}|\chi_T, BG+FG)$. The actual model described by M (M>0) Gaussian models can be presented as Equation (3).

$$p(\vec{x}^{(t)}|\chi_T, BG+FG) = \sum_{m=1}^{M} \omega_m \eta(\vec{x}; \vec{\mu}_m \sigma_m^2, I) \tag{3}$$

In Equation (3), ω_m is the weight of the mth Gaussian model, μ_m represents the average, and σ_m denotes the standard deviation. The independent relationship between the variables is assumed to simplify the calculation of the inverse matrix to prevent irreversible situation, and at this time, the covariance matrix is diagonal matrix. Gaussian probability density function η can be expressed as Equation (4).

$$\eta(\vec{x}; \vec{\mu}_m \sigma_m^2 I) = \frac{1}{(2\pi)^{\frac{n}{2}} \left|\sigma^2 I\right|^{\frac{1}{2}}} e^{-\frac{1}{2}(\vec{x}-\vec{\mu}_m)^T(\sigma^2 I)^{-1}(\vec{x}-\vec{\mu}_m)} \tag{4}$$

The recursive equations for parameter update of $\vec{x}^{(t)}$ of a new Gaussian mixture model at t time are shown in following equations.

$$\omega_m^{(t)} = \omega_m^{(t-1)} + \alpha(o_m^{(t)} - \omega_m^{(t-1)}) \tag{5}$$

$$\vec{\mu}_m^{(t)} = \vec{\mu}_m^{(t-1)} + o_m^{(t)}(\alpha/\omega_m^{(t)})\vec{\delta}_m^{(t)} \tag{6}$$

$$(\sigma_m^{(t)})^2 = (\sigma_m^{(t-1)})^2 + o_m^{(t)}(\alpha/\omega_m^{(t)})(\vec{\delta}_m^{(t)T}\vec{\delta}_m^{(t)} - (\sigma_m^{(t)})^2) \tag{7}$$

In Equation (5), α is the learning rate. When a new sample is judged as the background, $o^{(t)}$ equals 1; otherwise, the value of $o^{(t)}$ is 0. An essential parameter in the Gaussian mixture model is the learning rate α. If the speed of background updating increases with the growth of α, the system will quickly adapt to the change of the scene. However, there will be a phenomenon that the foreground and the background of slowly moving objects cannot be detected. On the contrary, when the speed of background updating slows with the decrease of α, the foreground of slowly moving objects can be detected, but the system cannot adapt to the scene's speed of change. A criterion is then introduced to determine whether the new sample belongs to the background, i.e., whether the Mahalanobis distance from the sample to the Gaussian model is less than 3σ, as shown in Equation (8).

$$\left|\vec{x}^{(t)} - \vec{u}_m^{(t-1)}\right| < 3\sigma_m \tag{8}$$

If one of the M Gaussian models fits the above criterion, the new sample belongs to the background. Otherwise, another Gaussian model is required, with the initialization parameter ω_{M+1} set as α and μ_{M+1} as $\vec{x}^{(t)}$, and $\sigma_{M+1} = \sigma_0$ means a given initial standard deviation. If M exceeds the number of specific Gaussian models, the smallest Gaussian model will be deleted. The moving foreground is generally represented by a Gaussian model with a smaller weight, so B Gaussian models with the most enormous weight are used to describe approximately the background, as expressed in Equation (9) and Equation (10).

$$p(\vec{x}^{(t)}|\chi_T, BG) \approx \sum_{m=1}^{B} \omega_m \eta(\vec{x}; \vec{\mu}_m \sigma_m^2, I) \tag{9}$$

$$B = \arg\min_b \left(\sum_{m=1}^{b} \omega_m > (1 - c_f)\right) \tag{10}$$

If the background model is not affected, a sample contains the maximum proportion of the foreground. Previous researchers made some adjustments to the update of the weight ω_m, as shown in Equation (11).

$$\omega_m = \omega_m + \alpha(o_m^{(t)}) - \omega_m) - \alpha c_T \tag{11}$$

In Equation (11), c_T is a smaller constant with a general value of 0.01. After updating ω_m, normalization is used to ensure that the sum of ω_m is 1. Besides, the Gaussian models with a negative value of ω_m are excluded to dynamically update the number of Gaussian models.

When the rotation matrix R and translation matrix T of the right camera relative to the left camera is sure, there are two methods to solve the three-dimensional coordinates of a point in the space [23]. The technique used here is correction first and calculation second. Through stereo correction and picture line alignment of the left and right cameras, three-dimensional coordinates are quickly obtained through multi-point stereo matching based on the parallax principle [24]. Figure 2 reveals the construction process of the three-dimensional trajectory.

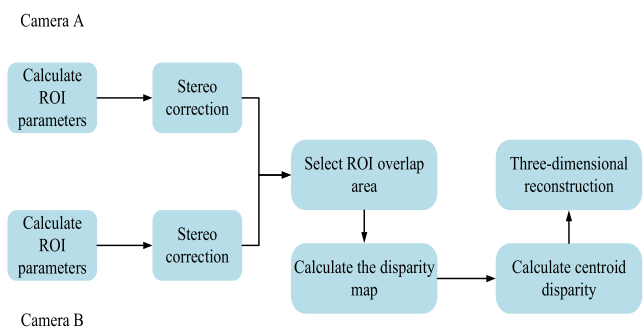

FIGURE 2. The construction process of three-dimensional trajectory.

It is necessary to track and predict the moving trajectory of badminton to solve the problem of time and position in the process of badminton movement. The initial position and velocity of the moving badminton can be obtained through multiple trajectory tracking, followed by trajectory prediction [25]. Due to the limitations of mechanical strength, motor power, and so on, badminton robots should predict the landing point of badminton to reserve sufficient time for the following position change [26], [27]. Figure 3 displays the trajectory tracking and prediction process of the badminton robot.

OpenGL (Open Graphics Library) is used to draw complex three-dimensional images, and GLUT (OpenGL Utility Toolkit) is used to illustrate the three-dimensional badminton

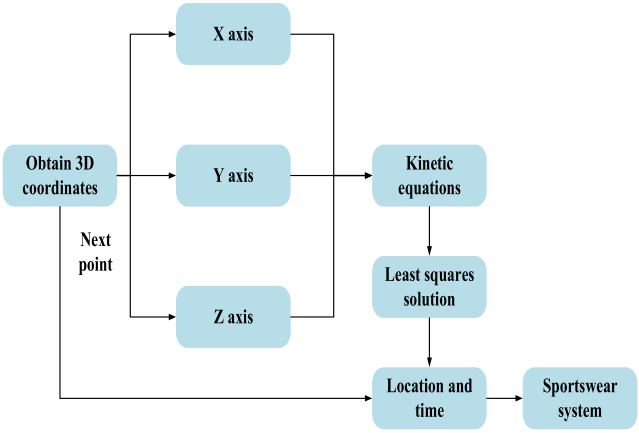

FIGURE 3. The flow path of trajectory tracking and prediction.

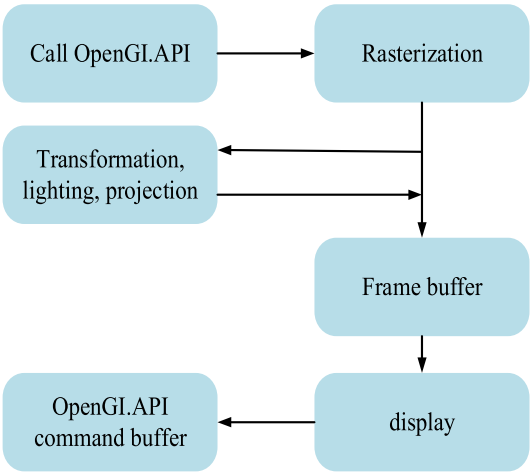

FIGURE 4. Basic drawing process of OpenGL.

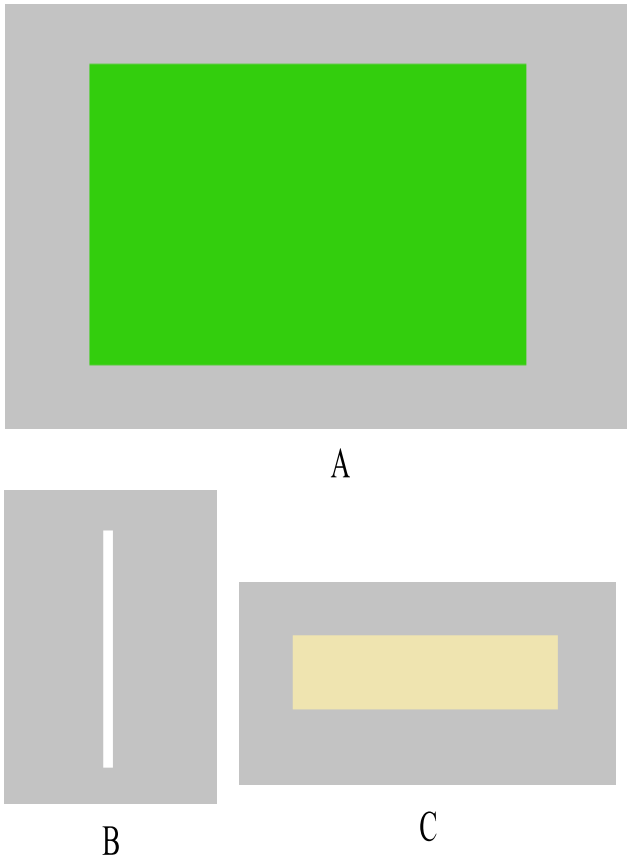

FIGURE 5. Three-dimensional model of the badminton court. (A: filed; B: net set; C: court fence).

court and continuously display the badminton trajectory [28], [29]. The function in OpenGL sends the command of drawing graphics to the command buffer, where the data performs some operations such as transformation, illumination, and projection. Ultimately, the data begins the rasterization process [30]. After that, the rasterization results are sent into the frame buffer, and the image will appear on the screen. Figure 4 presents the basic drawing process for OpenGL.

The badminton court is divided into three essential elements, including the field, badminton net set, and court fence to facilitate the three-dimensional rendering. After the three elements are basically drawn successfully, they are combined into a complete three-dimensional badminton court through a series of operations such as translation and rotation. Three-dimensional models of the three elements are shown in Figure 5.

III. DESIGN OF REAL-TIME POSITION MEASUREMENT FOR BADMINTON ROBOTS

A. BRIEF INTRODUCTION OF THE LASER MEASUREMENT SYSTEM (LMS221)

The Laser measurement system has the advantages of high resolution, strong anti-interference ability, and accurate ranging. Before using LMS221 (a laser measurement system), it is necessary to set the hardware and software, use a new baud rate to communicate with LMS221, and set its scanning angle and angular resolution [31], [32]. After the setting, continuous data requests are sent to LMS221 to output original data for further processing [33], [34]. Before resetting the parameters of LMS221, the stop command must be sent to the data transmission to prevent the data transmission confusion [35]. Figure 6 signifies the data processing process of LMS221.

Figure 6 shows the execution process of the motion mechanism of the badminton robot. According to Figure 6, the sub-thread is mainly responsible for the analysis and extraction of data flow and the test of measurement data. In the Windows API (Application Programming Interface) serial programming, the data is read or written asynchronously in the serial port because it has the advantages of simultaneous reading and writing data in the background efficiently. There are inevitable measurement errors since the realistic environment, instruments, and the technical level of the experimental personnel cannot be ideal. In contrast, the measurement experiment is carried out under fixed conditions. Therefore, the measurement errors are studied to reduce the measurement error data to a large extent to improve the accuracy of experimental measurement.

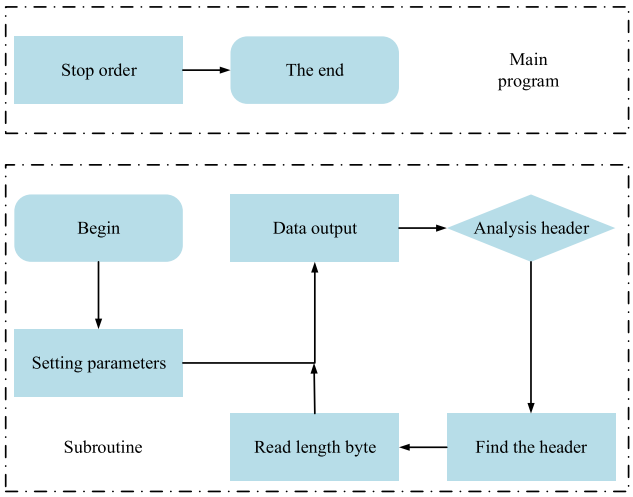

FIGURE 6. Data processing of LMS221.

B. MOTION CONTROL DESIGN OF BADMINTON ROBOT BASED ON IoT

IoT technology realizes the motion control of badminton robot is primarily through the CAN (controller area network). CAN transmits information to the universal wheel through the cooperation of multiple servo controllers, direct current reduction motors, and encoders, and finally feeds back to the badminton racket.

Figure 7 demonstrates the execution process of the movement mechanism of the badminton robot.

The collected image information is analyzed and judged by the computer. Then, the corresponding instructions are given to the badminton racket to convert the visual image into the corresponding action. The main task of the badminton robot's motion mechanism is to move to the specified position timely and accurately according to the command of the visual system and the feedback of the positioning system and then complete the hitting [36]. The researchers studied the PID (Proportion Integral Differential) model, which constructs the controlled quality through a linear combination of the deviation, integral, and differential of the proportion. When the proportional coefficient K_P is 0.3 and the integral coefficient K_I is 0.5, the badminton robot achieves a better control effect. Figure 8 shows the control model of the experiment.

C. EXPERIMENTAL SOFTWARE DESCRIPTION AND EXPERIMENTAL ENVIRONMENT CONFIGURATION

1) EXPERIMENTAL SETUP

The experiment is conducted within a robust hardware environment and accompanied by comprehensive software configuration, collectively underpinning the functionality of the intelligent real-time image processing system integrated with the badminton robot. The hardware selection involves an industrial-grade digital camera with specifications encompassing a resolution of 1280 × 960, pixel dimensions of 3.75 × 3.75 millimeters, and a steady frame rate of 40 frames per second. This camera is equipped with 128 MB of frame memory and featured an 8-bit data depth. Operationally, the camera harnesses the frame exposure mode to ensure optimal image clarity, even during rapid and high-speed motions. In terms of computational resources, the setup encompasses an Intel Core i5 4590 CPU (Central Processing Unit) clocked at 3.3 GHz. This is harmonized with a 64-bit Windows 7 operating system, and the development environment was facilitated through Visual Studio 2013.

2) EXPERIMENTAL PROCEDURE

The experimental protocol follows a systematic procedure to gather image data pertaining to the dynamic movements of the badminton shuttlecock. The utilization of frame exposure mode within industrial digital cameras facilitates the capture of high-quality images even in the presence of swift motion. Subsequent to image acquisition, a binocular stereo vision acquisition system undertook the analysis, leveraging machine vision techniques for image processing and decomposition. Processed image data are then transmitted to the computer system for subsequent rounds of image processing and comprehensive analysis. The motion control module synthesizes positional and postural commands based on the processed data. These commands steer the actions of the badminton robot, orchestrating hitting and maneuvering.

3) EXPERIMENTAL METRICS

The experiment relies on a repertoire of evaluation metrics to affirm the efficacy of the experimental outcomes. The assessment spectrum encompasses variables such as the recognition rate of the badminton robot, the standard deviation characterizing posture angles, and the standard deviation pertaining to position. These metrics enable a multi-faceted analysis of the binocular stereo vision acquisition system's accuracy, the Gaussian mixture model's precision in detecting minute and vulnerable motion targets, as well as the matching accuracy intrinsic to the Retinex-based color histogram matching method. Furthermore, the present work undertakes a comparative analysis between the developed algorithm and existing robot algorithms. This endeavor illuminates the comparative advantages and promising prospects that the experimental approach brings to the table in the evolution of the badminton robot.

The resolution of the industrial digital camera used in this experiment is 1280 × 960, the pixel size is 3.75 × 3.75, the frame rate is 40 fps, the frame memory is 128 MB, the data bit is 8 bits, and the exposure mode is frame exposure. The main configuration of the computer used in this experiment is as follows: CPU is Intel core i5 4590, the main frequency is 3.3 GHz, the operating system is 64-bit Windows7, and the development environment is Visual Studio 2013.

Fig. 8 illustrates how the badminton robot decomposes after collecting the image, which is the transformation from the visual system to motion control. Fig. 9 reveals the corresponding instructions for the position and attitude of the

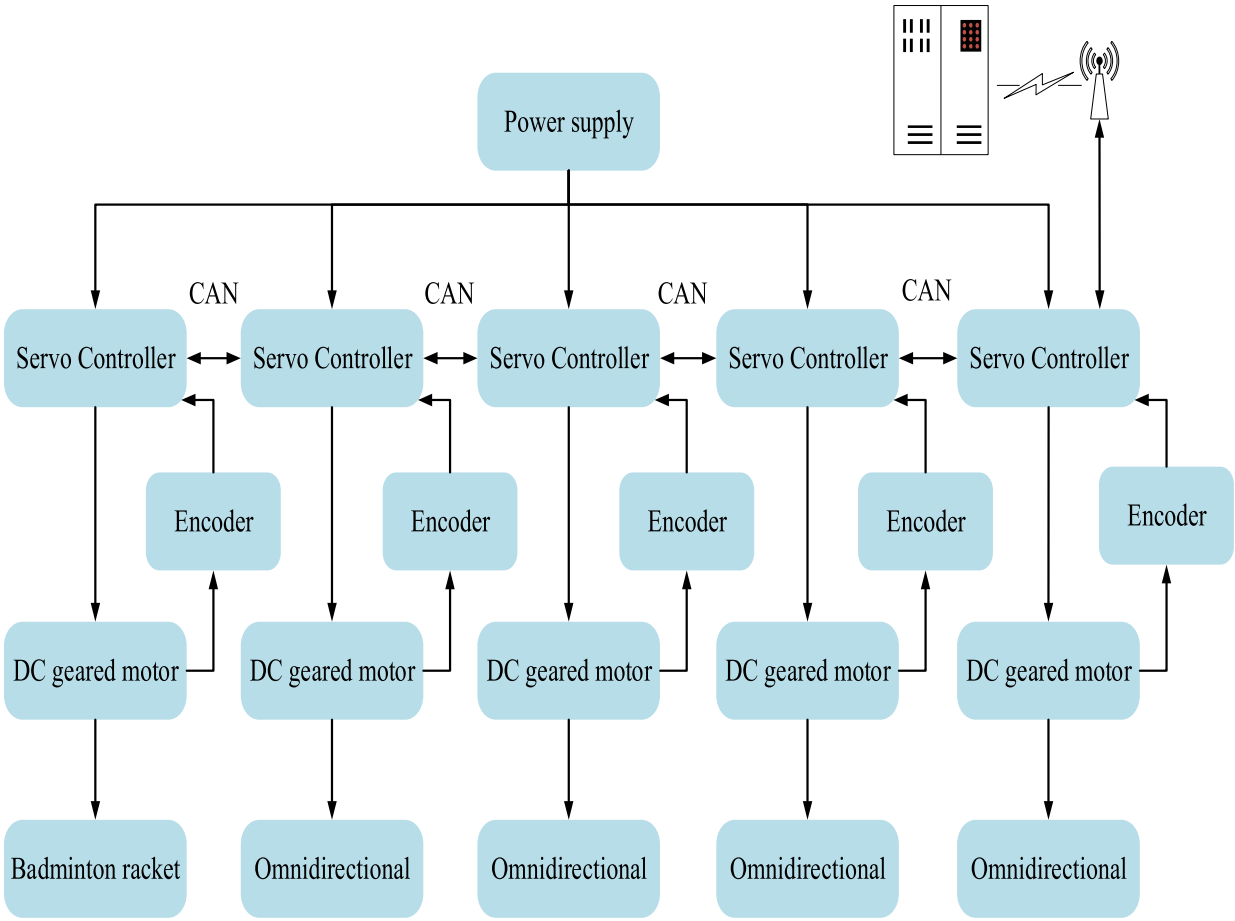

FIGURE 7. Execution process of badminton robot's movement mechanism.

badminton robot according to the motion control information in Figure 8.

IV. EXPERIMENTAL RESULTS

A. ANALYSIS OF CALIBRATION ERROR RESULTS

Figure 9 presents the analysis of calibration error results.

According to the comparison between the first calibration errors and the secondary calibration errors in Figure 10, the secondary calibration errors are more closely distributed around 0 with a more minor variance, indicating that the secondary calibration has higher accuracy. The semi-automatic calibration method proposed by Zhang Zhengyou is adopted in the experiment. The experimental results show that Zhang's calibration method is feasible, and it can satisfy the accuracy of this system.

B. ANALYSIS OF THRESHOLD SEGMENTATION RESULTS

Figure 10 provides the image processing result of a frame in the video.

By comparing Figure 10-A and Figure 10-B, white objects like white walls with similar colors to the shuttlecock is marked as yellow or red by the system. Besides, the location judgment of a bit of sunlight is entirely accurate, consistent with the position of the shadow. The parts with different colors from the shuttlecock in the background are marked as blue. Therefore, similar objects can be accurately distinguished by avoiding the interference of sunlight illumination through the feature vector based on SVD.

C. COMPARATIVE ANALYSIS OF DETECTION RESULTS

In Figure 11, the color of the shuttlecock is exceptionally different from the background, and the detection results of the two Gaussian models are almost the same. However, when the color difference is negligible between the background and the shuttlecock, as shown in Figure 12, the general Gaussian mixture model cannot detect the high-speed shuttlecock at the moment. In contrast, the proposed model can still detect the shuttlecock precisely.

The characteristics of the extracted motion foreground have to be matched to those of the specific targets to ensure accurate detection. The homomorphic filtering is adopted to estimate the sunlight intensity of each part of the image to match the appropriate color histogram template to improve the accuracy of color matching. Figure 13 shows the color histograms of the shuttlecock in the medium illumination intensity area and low illumination intensity area.

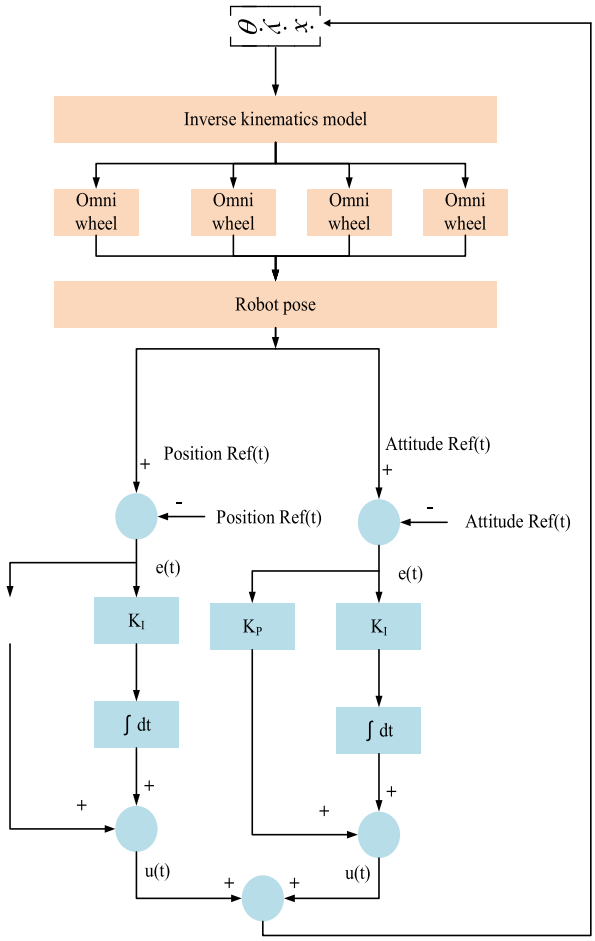

FIGURE 8. A framework of the control model.

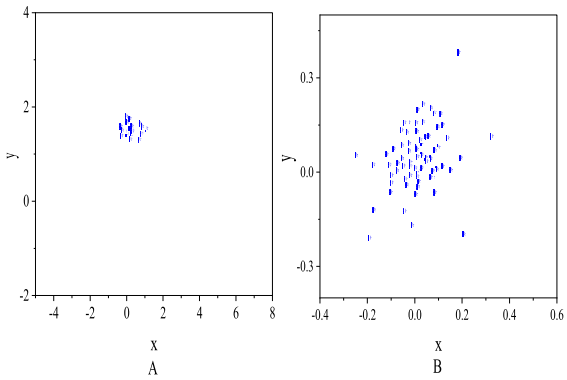

FIGURE 9. Results of calibration errors. (A: the first calibration errors; B: the secondary calibration errors).

Figures 13 shows color histograms of the shuttlecock in medium illumination areas and low illumination areas, respectively. The Mahalanobis distance of the color histograms is 0.5991, while the Mahalanobis distance is 0.3902 by using the proposed model, which is more practical in reality.

Figure 14 describes the images of three frames in the video.

During the detection of moving dim small targets, the down-sampling operation is conducted on cameras reducing the resolution to 320 × 240 to improve the operation speed and ensure real-time performance. The left column and right

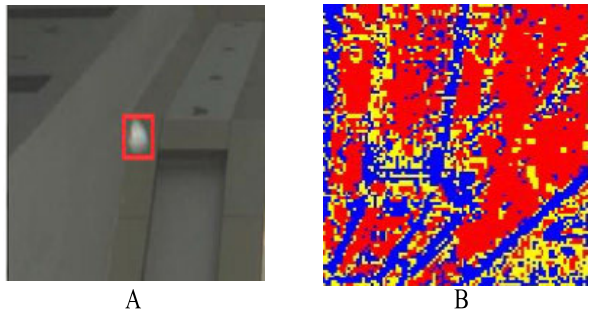

FIGURE 10. Image processing result of a frame in the video (A: the frame; B: image processing result).

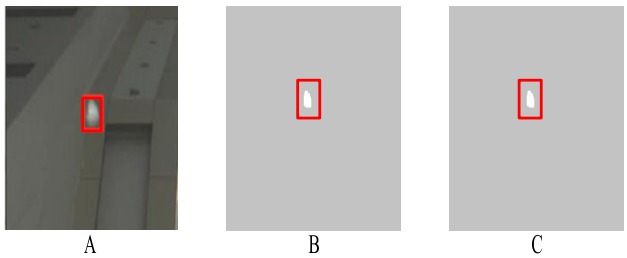

FIGURE 11. Comparison 1 (A: a frame in the video; B: detection result of the general Gaussian mixture model; C: detection result of the proposed Gaussian mixture model).

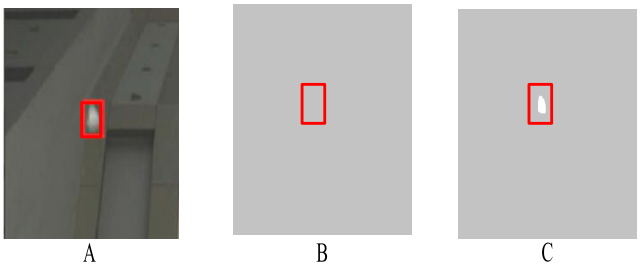

FIGURE 12. Comparison 2 (A: a frame in the video; B: detection result of the general Gaussian mixture model; C: detection result of the proposed Gaussian mixture model).

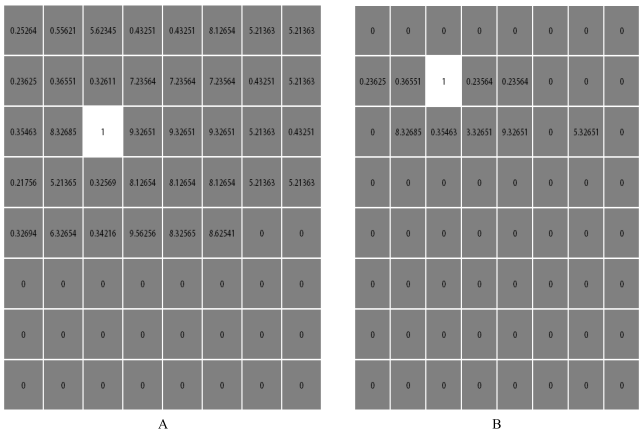

FIGURE 13. Color histograms of the shuttlecock. (A: in medium illumination intensity areas; B: in low illumination intensity areas).

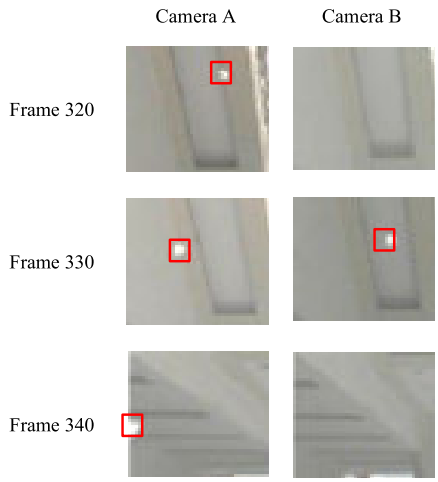

FIGURE 14. Images of three frames of the video.

-1	-1	-1	-1	-1	-1	-1	-1
-1	-1	-1	-1	-1	-1	-1	-1
-1	-1	-1	-1	-1	-1	-1	-1
-1	-1	-1	-1	-1	-1	-1	-1
-1	-1	-1	-1	-1	-1	-1	-1
-1	-1	-1	-1	-1	-1	-1	-1
-1	-1	-1	-1	-1	-1	-1	-1
-1	-1	-1	-1	-1	-1	-1	-1

FIGURE 15. Calculation results of the parallax error.

column in Figure 15 are the images captured by the left camera and the right camera, respectively. It is obvious that from the 320th frame, both the left camera and right camera can detect the shuttlecock. By comparing the left column and right column of the same row, there is a significant difference between images of the left camera and the right camera.

The calculation results of the parallax error are shown in Figure 15.

From Figure 15, the calculation results of the parallax error of most regions are -1. The actual parallax error should be the sum of -1 and the error value in the x-axis direction of two Regions of Interest, 243. The calculation shows that the position of the shuttlecock is 1953.2 mm away from the visual system in the depth direction, which coincides with the actual situation.

D. ANALYSIS OF MEASUREMENT ERROR RESULTS

Figure 16 shows the results of measurement errors.

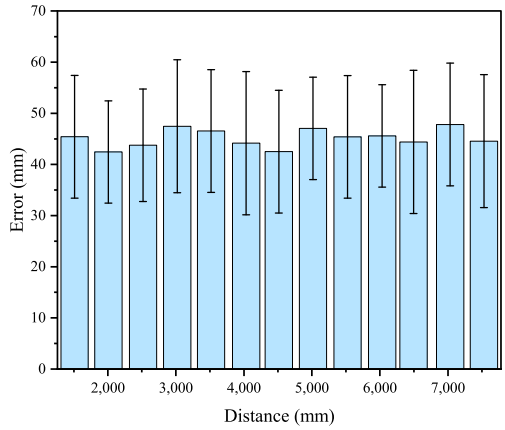

FIGURE 16. Results of measurement errors.

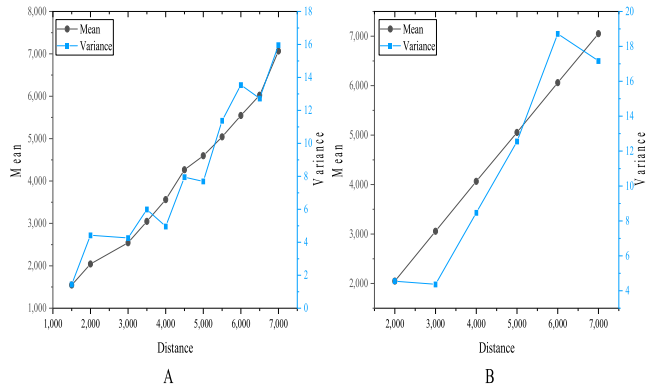

FIGURE 17. Ranging results (A: the mean and variance of the measuring distance; B: measuring distance on the surfaces with different materials).

In Figure 16, the mean variation of measurement results is distributed in the range of 40mm to 49mm, mainly caused by the fact that the starting point of the measurement ruler is not coincident with the laser radar origin. Therefore, the average deviation can be eliminated through the origin correction, after which the results of measurement error range from -14mm to 14 mm. Moreover, the measurement error expands with the increase of distance.

Figure 17 denotes the ranging results.

Figure 17A portrays the collective variance in measured distances, revealing subtle oscillations primarily clustered around the mean value. With the augmentation of distance, the variance progressively widens. Conversely, Figure 17B illustrates the mean fluctuations in measurements captured on the aluminum plate, consistently confined within the 40mm to 49mm range. Notably, these measurement points closely cluster around the mean, attesting to a remarkable uniformity in measurement outcomes. By contrasting Figure 18A with Figure 18B, the discernible impact of the primary aluminum plate and the alumina plate on the LMS221 lidar measurements comes into view. The ramifications of these distinct surface materials on the measurements are constrained, reinforcing that the consideration of measurement errors due to

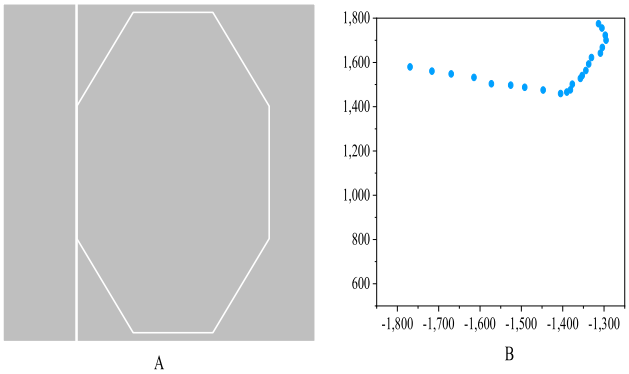

FIGURE 18. The model constructed by Matlab and the measurement results of LMS221. (A: the model; B: simulation data).

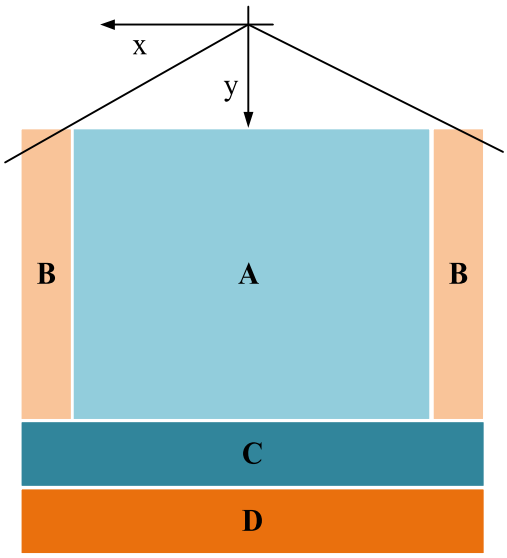

FIGURE 19. Activity partition of the badminton robot.

varying surface materials is unwarranted in the context of the badminton robot's position measurement.

Figure 18 shows the model constructed by Matlab and the ranging results of LMS221.

The model constructed by Matlab is shown in Figure 19A. The right-hand system is established by taking the laser radar as the origin. Each laser pulse is emitted from the origin of coordinates and is rotated and translated into the badminton robot model to obtain the simulation information of LMS221 under different poses. The translation vector of the badminton robot is 57 positions, generating 789 sets of simulation data.

The activity partition of the badminton robot is presented in Figure 19.

Figure 19 illustrates the delineation of the operational space within which the badminton robot functions, partitioned into distinct Zones labeled as A, B, C, and D. All these zones share a common coordinate origin and LIDAR origin. Zone A assumes a central role as the primary operational domain for the badminton robot, closely followed by Zone C in significance. In contrast, Zone B occupies the outer

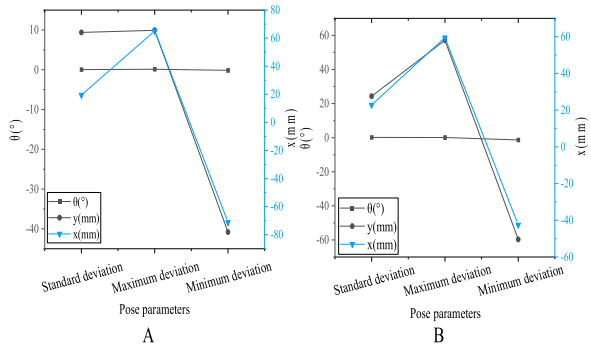

FIGURE 20. Calculation results of positions in Zone A (A: the first situation; B: the second situation).

boundaries of the badminton court, while Zone D situates itself proximate to the court's fencing. Notably, the robot's engagement in Zone D is relatively sporadic. Each zone is further characterized by two specific conditions, predicated on the angle (θ value) and the prevailing status of the robot. Predominantly, the angle lies within the range of $-30 \leq \theta \leq 30$, with a minority of cases wherein θ falls below -30 or surpasses 30.

The calculation results of positions are shown in Figure 20 to Figure 23.

Figures 20 to 23 facilitate a comparative assessment of detection rates and measurement precision within the context of the four delineated zones under the two distinct conditions. A discernible pattern emerges, highlighting the algorithm's superior performance within Zones A and C, in contrast to Zones B and D. Furthermore, detection rates and measurement accuracy prove higher under the first condition in comparison to the second. This discrepancy largely stems from the constrained angular resolution of the LIDAR's emitted laser pulses, rendering precise boundary measurements of the robot a challenging endeavor. Moreover, the incremental elevation of distance and pose angle correlates with an amplified measurement error. In summation, the model establishes a heightened detection rate and positional measurement precision within the customary operational spectrum of the badminton robot while also substantiating its capacity for accurate robot displacement across alternative zones.

E. ANALYSIS OF RESULTS OF THE HITTING EXPERIMENT

Figure 24 shows the moving trajectory of the shuttlecock.

Figure 24 is the moving trajectory of the shuttlecock, where Figure A and Figure B represent the moving trajectory before filtering and after filtering, respectively. Through comparative analysis, the extended Kalman filter can smooth the trajectory and converge rapidly. The coordinates in the figure are the original coordinates of the shuttlecock in the three-dimensional space obtained from the parallax calculation of the left and right cameras of each frame image and the coordinates obtained through the extended Kalman filter. The original data of the x-axis changes hugely, while the data information of the y-axis and the z-axis is relatively stable.

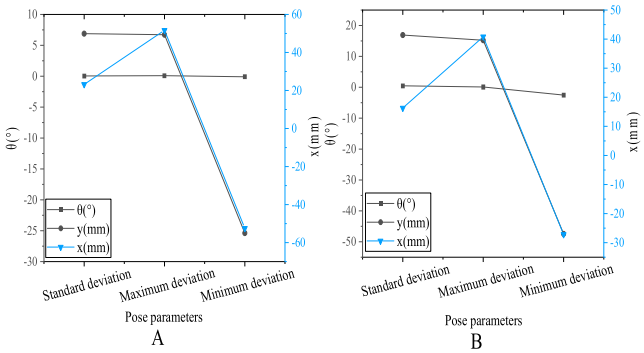

FIGURE 21. Calculation results of positions in Zone B (A: the first situation; B: the second situation).

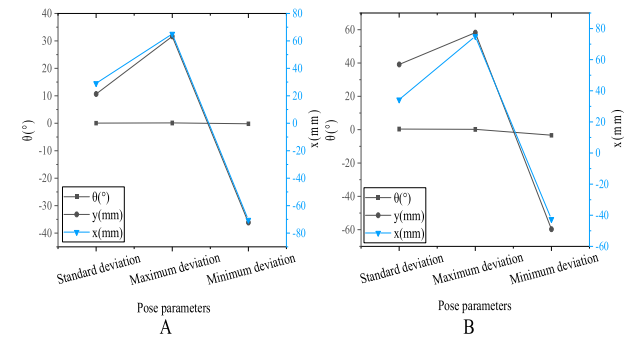

FIGURE 22. Calculation results of positions in Zone C (A: the first situation; B: the second situation).

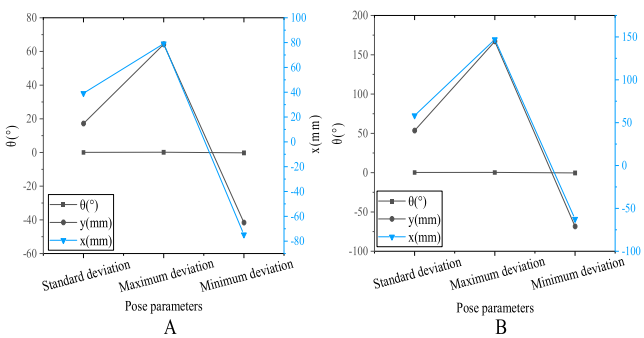

FIGURE 23. Calculation results of positions in Zone D (A: the first situation; B: the second situation).

Comparing the data of the x axis before and after filtering, the original data of the 314th frame, the 315th frame, and 316th frame are not quite in line with the reality, which is caused by the influence of noise and measurement accuracy. The extended Kalman filtering can effectively improve this phenomenon.

F. IMPLEMENTATION AND VERIFICATION OF SHUTTLECOCK TRACKING ALGORITHM

Figure 25 illustrates the predicted results of the shuttlecock trajectory.

From Figure 25, there is a significant deviation between the first trajectory prediction and the actual trajectory. During

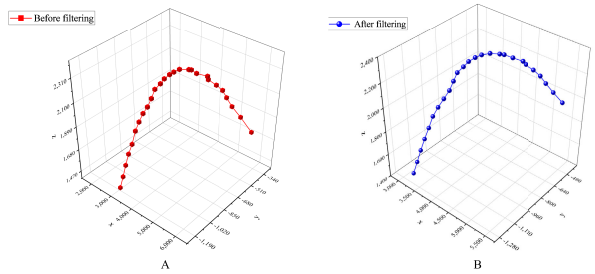

FIGURE 24. Moving trajectory of the shuttlecock (A: before filtering; B. after filtering).

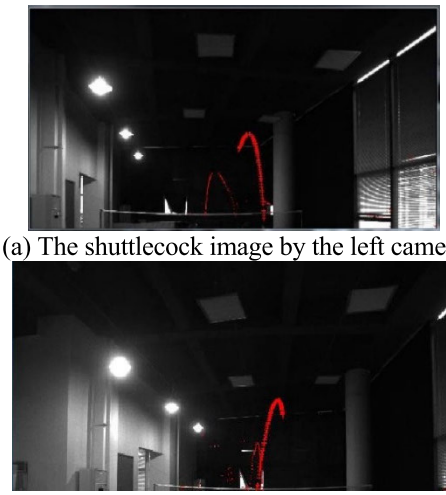

(a) The shuttlecock image by the left camera

(b) The shuttlecock image by the right camera

FIGURE 25. Predicted trajectory of shuttlecock.

the flight process, the flight state is corrected and updated through the measured value, and the predicted shuttlecock trajectory is increasingly close to the actual trajectory.

G. COMPARISON BETWEEN ALGORITHMS

Under the same experimental conditions, this badminton robot is compared with the badminton robots proposed by Chen et al. [8] and Mori et al. [7]. The technical means used by Chen et al. was a fast target center tracking method (FTOC) integrating heterogeneous clues with the AdaBoost algorithm, which was superior in solving the tracking problem in challenging scenes such as scale change and background clutter. Mori et al. developed a humanoid robot arm. They realized the complex degree of freedom and large-scale motion by reducing the overall weight using the actuator as the connecting rod structure. In this experiment, the badminton robot reported here moves in Region A of Figure 20. Under the first state, the recognition rate of the shuttlecock is 100%, the SD of attitude angle θ is less than 0.05°, the SD of position in the x-axis direction is less than 18 mm, and the SD of position in the y-axis direction is less than 8 mm. Under the same conditions, the recognition rate of shuttlecock by the robot proposed by Chen et al. is 92%, and the SD of attitude angle θ is less than 0.35°. In addition,

TABLE 1. Overall performance of the badminton robot.

Experiment Number	Time for Motion Trajectory Determination	Time from Specific Position to Target Position	Ability to Reach Target Before Badminton robot Estimated Decision and Motion Time (seconds)	Estimated decision and movement time (seconds)
1	0.52	0.78	Yes	0.78
2	0.47	0.65	Yes	0.65
3	0.61	0.82	Yes	0.82

under the same conditions, the recognition rate of shuttlecock by the robot developed by Mori et al. is 96%, and the SD of attitude angle θ is less than 0.15°. Obviously, this algorithm has a higher recognition rate than that proposed by Chen et al. and Mori et al., with a lower attitude angle than that developed by Chen et al. and Mori et al.

H. EVALUATION OF BADMINTON ROBOT'S PERFORMANCE

Multiple simulation experiments have been meticulously conducted, yielding the comprehensive performance outcomes of the badminton robot, as summarized in Table 1.

Table 1 presents results that reveal the average time required for determining the badminton trajectory falls within the range of 0.52 to 0.61 seconds. The time range for moving from a specific position to the target is recorded between 0.65 and 0.82 seconds. Traditionally, estimated decision and motion times were obtained by summing trajectory determination and motion time. However, in this work, decision and motion time now represent the maximum values of the two aforementioned components. This result signifies that this badminton robot has the capacity to simultaneously calculate decision time and motion decisions. To sum up, the design and algorithm reported here exhibit remarkable capabilities in both the motion control and decision-making aspects of the badminton robot, thereby providing a robust foundation for further advancements in this field.

I. DISCUSSION

This work delves into the realm of intelligent real-time image processing for badminton robots, leveraging IoT technology. The analysis of the experimental results underscores the affirmative strides made in the domain of intelligent image processing for badminton robots. The integration of an IoT-facilitates binocular stereo vision acquisition system and the Retinex-based color histogram matching method has provided a high-precision foundation for real-time image processing within the robot's operations.

Although specific scenarios do present inherent limitations in detection rates and measurement precision, the model has demonstrated commendable overall performance within the customary operational scope of the badminton robot. This work enriches the technological trajectory of badminton robots and offers pragmatic solutions for real-world application scenarios. Confidence is held in the forthcoming development of intelligent badminton robots, and these achievements are poised to infuse a new dynamism into their evolutionary path.

V. CONCLUSION

IoT is an information carrier based on the internet and traditional telecommunication networks. Through various possible network access, it realizes the ubiquitous connection between things and people, and achieves the intelligent perception, identification, and management of things and processes. An intelligent real-time image processing system is constructed here for badminton robots. A high-precision binocular stereo vision acquisition system is adopted based on the machine vision technology of the IoT aiming at the real-time detection and trajectory tracking prediction of specific moving dim small targets. Meanwhile, laser radar is responsible for estimating the real-time position of the shuttlecock. Finally, the experiment achieves the simple bating action of the badminton robot by machine vision technology based on IoT. The experimental results show that the binocular stereo vision acquisition system has high accuracy. The Gaussian mixture model for moving dim small targets also has a high detection accuracy by setting the threshold according to the similarity of background and foreground. Based on the color histogram matching method of Retinex, different color histogram templates are set according to different illumination intensities to improve the accuracy of matching.

The research is conducted under novel technologies and substantial data, but there are still some shortcomings that need to be improved. In terms of image processing, this experiment only detects the flying ball in a simple indoor environment. In contrast, the outdoor environment has more complex changes in the background and light intensity, which is also the future research direction. In terms of intelligent decision-making and servo control, path planning will be taken into consideration to design a multi-degree-of-freedom badminton robot flapping system, derive the forward and inverse kinematics of the model, and select the appropriate motion planning algorithm.

REFERENCES

[1] N. Mizuno, T. Makishima, K. Tsuge, S. Kondo, T. Nonome, H. Kurebayashi, S. Otake, D. Shibata, and S. Yamakawa, "Development of automatic badminton playing robot with distance image sensor," *IFAC-PapersOnLine*, vol. 52, no. 8, pp. 67–72, 2019.

[2] S. Yang, "Research on development patterns of youth sports clubs in Fuzhour–Taking Fujian ShengYu international badminton club as an example," *Sport/Sci. Sports*, vol. 21, no. 3, pp. 56–58, Jun. 2017.

[3] E. Ugur, Y. Nagai, E. Sahin, and E. Oztop, "Staged development of robot skills: Behavior formation, affordance learning and imitation with motionese," *IEEE Trans. Auto. Mental Develop.*, vol. 7, no. 2, pp. 119–139, Jun. 2015.

[4] G. Jiang, G. Li, J. Kong, Y. Sun, Z. Li, and H. Liu, "Development of articulated robot trajectory planning," *Int. J. Comput. Sci. Math.*, vol. 8, no. 1, p. 52, 2017.

[5] H. Yu, I. S. Choi, K.-L. Han, J. Y. Choi, G. Chung, and J. Suh, "Development of a upper-limb exoskeleton robot for refractory construction," *Control Eng. Pract.*, vol. 72, pp. 104–113, Mar. 2018.

[6] T. Taniguchi, T. Nishimura, M. Hammadi, J.-Y. Choley, A. Ming, and M. Shimojo, "Development of biomimetic soft underwater robot," *Trans. Soc. Instrum. Control Eng.*, vol. 55, no. 4, pp. 252–259, 2019.

[7] S. Mori, K. Tanaka, S. Nishikawa, R. Niiyama, and Y. Kuniyoshi, "High-speed humanoid robot arm for badminton using pneumatic-electric hybrid actuators," *IEEE Robot. Autom. Lett.*, vol. 4, no. 4, pp. 3601–3608, Oct. 2019.

[8] W. Chen, T. Liao, Z. Li, H. Lin, H. Xue, L. Zhang, J. Guo, and Z. Cao, "Using FTOC to track shuttlecock for the badminton robot," *Neurocomputing*, vol. 334, pp. 182–196, Mar. 2019.

[9] P. Rodríguez-Gonzálvez, M. Rodríguez-Martín, L. F. Ramos, and D. González-Aguilera, "3D reconstruction methods and quality assessment for visual inspection of welds," *Autom. Construct.*, vol. 79, pp. 49–58, Sep. 2017.

[10] N. Jia, Z. Li, J. Ren, Y. Wang, and L. Yang, "A 3D reconstruction method based on grid laser and gray scale photo for visual inspection of welds," *Opt. Laser Technol.*, vol. 119, Nov. 2019, Art. no. 105648.

[11] A. Gorevoy and A. Machikhin, "Optimal calibration of a prism-based videoendoscopic system for precise 3D measurements," *Comput. Opt.*, vol. 41, no. 4, pp. 535–544, 2017.

[12] J. Li, Y. Tang, X. Zou, G. Lin, and H. Wang, "Detection of fruit-bearing branches and localization of litchi clusters for vision-based harvesting robots," *IEEE Access*, vol. 8, pp. 117746–117758, 2020.

[13] Q. Guo, Y. Chen, Y. Tang, J. Zhuang, Y. He, C. Hou, X. Chu, Z. Zhong, and S. Luo, "Lychee fruit detection based on monocular machine vision in orchard environment," *Sensors*, vol. 19, no. 19, p. 4091, Aug. 2019.

[14] M. Chen, Y. Tang, X. Zou, Z. Huang, H. Zhou, and S. Chen, "3D global mapping of large-scale unstructured orchard integrating eye-in-hand stereo vision and SLAM," *Comput. Electron. Agricult.*, vol. 187, Aug. 2021, Art. no. 106237.

[15] Z. Song, Z. Zhou, W. Wang, F. Gao, L. Fu, R. Li, and Y. Cui, "Canopy segmentation and wire reconstruction for kiwifruit robotic harvesting," *Comput. Electron. Agricult.*, vol. 181, Feb. 2021, Art. no. 105933.

[16] Y. Tang, Z. Huang, Z. Chen, M. Chen, H. Zhou, H. Zhang, and J. Sun, "Novel visual crack width measurement based on backbone double-scale features for improved detection automation," *Eng. Struct.*, vol. 274, Jan. 2023, Art. no. 115158.

[17] Y. Tang, M. Zhu, Z. Chen, C. Wu, B. Chen, C. Li, and L. Li, "Seismic performance evaluation of recycled aggregate concrete-filled steel tubular columns with field strain detected via a novel mark-free vision method," *Structures*, vol. 37, pp. 426–441, Mar. 2022.

[18] Z. Luo, K. Zhang, Z. Wang, J. Zheng, and Y. Chen, "3D pose estimation of large and complicated workpieces based on binocular stereo vision," *Appl. Opt.*, vol. 56, no. 24, p. 6822, Aug. 2017.

[19] Z. Cao, T. Liao, W. Song, Z. Chen, and C. Li, "Detecting the shuttlecock for a badminton robot: A YOLO based approach," *Exp. Syst. Appl.*, vol. 164, Feb. 2021, Art. no. 113833.

[20] Y. Tang, L. Li, C. Wang, M. Chen, W. Feng, X. Zou, and K. Huang, "Real-time detection of surface deformation and strain in recycled aggregate concrete-filled steel tubular columns via four-ocular vision," *Robot. Comput.-Integr. Manuf.*, vol. 59, pp. 36–46, Mar. 2019.

[21] M.-S. Wei, F. Xing, and Z. You, "A real-time detection and positioning method for small and weak targets using a 1D morphology-based approach in 2D images," *Light, Sci. Appl.*, vol. 7, no. 5, p. 18006, 2018.

[22] S. Shaikh, L. Changan, M. R. Malik, and M. A. Khan, "Software defect-prone classification using machine learning: A virtual classification study between LibSVM & LibLinear," in *Proc. 13th Int. Conf. Math., Actuarial Sci., Comput. Sci. Statist.*, Dec. 2019, pp. 1–6.

[23] S. Ahmed, S. Shaikh, F. Ikram, M. Fayaz, H. S. Alwageed, F. Khan, and F. H. Jaskani, "Prediction of cardiovascular disease on self-augmented datasets of heart patients using multiple machine learning models," *J. Sensors*, vol. 2022, pp. 1–21, Dec. 2022.

[24] A. Morozov, A. Popolitov, and S. Shakirov, "On (q,t)-deformation of Gaussian matrix model," *Phys. Lett. B*, vol. 784, pp. 342–344, Sep. 2018.

[25] S. Shaikh, L. Changan, and M. R. Malik, "Attribute rule performance in data mining for software deformity prophecy datasets models," in *Proc. Int. Conf. Adv. Emerging Comput. Technol. (AECT)*, Feb. 2020, pp. 1–6.

[26] S. Shaikh, L. Changan, and M. R. Malik, "A widely analysis & assessment of software deformity prone datasets models using LinearNNsearch classification model," in *Proc. IEEE Int. Conf. Commun., Netw. Satell.*, Oct. 2020, pp. 314–318.

[27] L. Cai, X. Tian, and S. Chen, "Monitoring nonlinear and non-Gaussian processes using Gaussian mixture model-based weighted kernel independent component analysis," *IEEE Trans. Neural Netw. Learn. Syst.*, vol. 28, no. 1, pp. 122–135, Jan. 2017.

[28] J. R. Doyle, P. A. Bottomley, and R. Angell, "Tails of the travelling Gaussian model and the relative age effect: Tales of age discrimination and wasted talent," *PLoS ONE*, vol. 12, no. 4, Apr. 2017, Art. no. e0176206.

[29] Z. Shi, M. Xu, and Q. Pan, "4-D flight trajectory prediction with constrained LSTM network," *IEEE Trans. Intell. Transp. Syst.*, vol. 22, no. 11, pp. 7242–7255, Nov. 2021.

[30] Y.-J. Lin and S.-K. Weng, "Trajectory estimation of the players and shuttlecock for the broadcast badminton videos," *IEICE Trans. Fundamentals Electron., Commun. Comput. Sci.*, vol. 101, no. 10, pp. 1730–1734, Oct. 2018.

[31] B. Yu, Z. Guo, S. Asian, H. Wang, and G. Chen, "Flight delay prediction for commercial air transport: A deep learning approach," *Transp. Res. E, Logistics Transp. Rev.*, vol. 125, pp. 203–221, Feb. 2019.

[32] K. Liu, D. Zhang, and J. F. Zhang, "Modeling and simulation of trajectory and destination prediction of objects drifting in inland waterways," *S. China Marit. Asia*, vol. 41, no. 4, pp. 62–63, Jun. 2018.

[33] X. Shen, Q.-Q. Li, G. Wu, and J. Zhu, "Decomposition of LiDAR waveforms by B-spline-based modeling," *ISPRS J. Photogramm. Remote Sens.*, vol. 128, pp. 182–191, Jun. 2017.

[34] M. Cheng, Z. Cai, W. Ning, and H. Yuan, "System design for peanut canopy height information acquisition based on LiDAR," *IS*, vol. 35, no. 1, p. 180, 2019.

[35] T. Palonen, H. Hyyti, and A. Visala, "Augmented reality in forest machine cabin," *IFAC-PapersOnLine*, vol. 50, no. 1, pp. 5410–5417, Jul. 2017.

[36] S. Mori, K. Tanaka, S. Nishikawa, R. Niiyama, and Y. Kuniyoshi, "High-speed and lightweight humanoid robot arm for a skillful badminton robot," *IEEE Robot. Autom. Lett.*, vol. 3, no. 3, pp. 1727–1734, Jul. 2018.